Benchmarks for Magnetic Field Aligned Meshes in Electromagnetic Plasma Thruster Simulations

IEPC-2015-203/ISTS-2015-b-203

Presented at Joint Conference of 30th International Symposium on Space Technology and Science, 34th International Electric Propulsion Conference and 6th Nano-satellite Symposium Hyogo-Kobe, Japan July 4–10, 2015

D. Pérez-Grande*, O. Gonzalez-Martinez, P. Fajardo and E. Ahedo†
Aerospace Engineering Group, Universidad Carlos III de Madrid, Spain

Keywords: Plasma Propulsion, Magnetic Field Aligned Mesh, Numerical Diffusion, Benchmarks

A short study on numerical errors for highly anisotropic diffusion problems in propulsion plasmas is presented in order to address the use of magnetic field aligned meshes versus regular structured meshes in numerical solutions. Numerical diffusion in structured meshes is quantified by solving the classical anisotropic diffusion problem. Meshing strategies and Gradient Reconstruction methods for magnetically aligned meshes are presented in order to provide insight into achieving acceptable mesh regularity. Numerical errors are compared for a benchmark problem on structured and magnetically aligned meshes. It is concluded that the latter provides a more correct approach to solving problems with anisotropicity, specially if anisotropicity levels are high or difficult to quantify.

I. Introduction

A typical assumption in the modeling of *electric propulsion plasmas* is that the electron population (which is generally the only one "magnetized", i.e., confined by the magnetic field) can be considered a maxwellian fluid of a highly anisotropic nature, in which transport in the perpendicular and parallel directions to the magnetic field is widely different. The equations which govern the evolution of the electron population can be solved in a curvilinear system of coordinates defined through the local magnetic field directions, as long as the magnetic field may be considered "static" (i.e., the magnetic field $\vec{B}$ can be assumed irrotational in addition to solenoidal and stationary); the numerical simulation mesh whose element facets are locally aligned with the magnetic field directions is called the Magnetic Field Aligned Mesh (MFAM), as shown in Fig. 1.

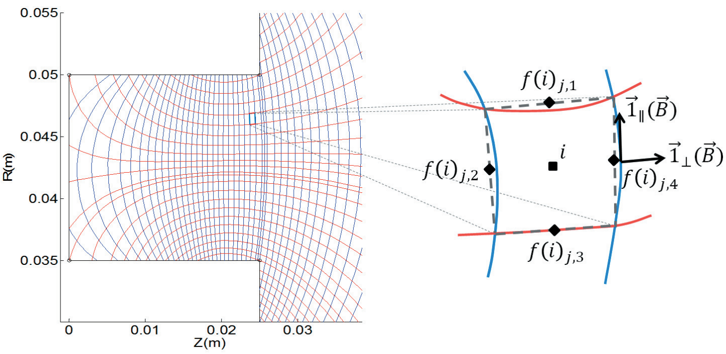

Figure 1. MFAM in an axisymmetric simulation domain for the SPT-100 HET & *detail* of Mesh element

*Correspondence Author @ daperezg@ing.uc3m.es
†Keynote Speaker

An added perk to discretizing the problem on the MFAM is that this approach helps to avoid "artificial" numerical diffusion plaguing the solution; indeed, because of the large anisotropicity in the electron transport coefficients for the parallel and perpendicular directions, solving the governing equations in a mesh which is *not* aligned with the magnetic field may lead to "cross-contamination" of the transport coefficients and thus to numerical diffusion (please refer to Section II). The MFAM venue has been utilized extensively both by the fusion plasma[1] and the plasma propulsion[2] communities, and numerical diffusion has been documented in simulations for highly anisotropic systems;[3,4] however, a number of difficulties may arise when using the MFAM, mainly in relation to low quality meshes, problematic boundary elements, calculation of gradients and the errors associated with them, as discussed by Araki.[5]

The EP2 Group[a] at UC3M, building from the expertise gained from the development of the HPHall-2 and HallMA codes,[6] is currently developing NOMADS (NOn-structured Magnetically Aligned plasma Discharge Simulation), an advanced platform for simulation of plasma discharges in various thruster configurations and magnetic field topologies. Specifically, NOMADS is aimed at solving plasma discharges in Hall Effect Thrusters -HETs- and derived HETs with non-regular magnetic field topologies: singular points, cusp regions, etc. For this, the electron population will be modeled as a bi-Maxwellian (non-isotropic Velocity Distribution Function), magnetized, fluid, and solved in the MFAM.

Following the discussion by Araki,[5] efforts have been carried out to justify using the MFAM as opposed to regular, structured, meshes. The present work tackles the issues of numerical diffusion in regular meshes and mesh quality and gradient reconstruction issues in non-structured meshes; additionally, a *benchmark* test is presented showcasing the benefits of using MFAMs versus structured meshes in anisotropic problems.

II. Numerical Diffusion in regular, structured, meshes: the anisotropic diffusion problem

The classical *anisotropic diffusion problem* in magnetized plasmas is well known: it is similar to the *ambipolar diffusion problem* (in which an ambipolar electric field is established to balance the fluxes of the electron and ion species), except that the parallel ($\|$) and perpendicular ($\perp$) transport coefficients account for the anisotropy of the problem and currents flowing in the direction of the magnetic field are responsible for space charge neutrality.

A formal derivation by Simon,[7] considering the quasineutrality $n_e \approx n_i = n$ assumption, for an infinite 2D slab with conducting walls under a straight magnetic field leads to Eq. (1):

$$\frac{dn}{dt} = \begin{bmatrix} \frac{\mu_e D_{i\perp} - \mu_i D_{e\perp}}{\mu_e - \mu_i} & 0 \\ 0 & \frac{\mu_e D_{i\|} - \mu_i D_{e\|}}{\mu_e - \mu_i} \end{bmatrix} \begin{bmatrix} \frac{\partial^2 n}{\partial x'^2} \\ \frac{\partial^2 n}{\partial y'^2} \end{bmatrix} \tag{1}$$

Where the μ terms are the mobility coefficients for both species and $D_\perp$ and $D_\|$ are, respectively, the diffusion across the magnetic field (which only accounts for classical collision mechanisms) and the "free" or natural diffusion coefficient (which appears in the non-confined direction parallel to the magnetic field); x' and y' are, respectively, the coordinates associated to the directions perpendicular ($\vec{1}_\perp$) and parallel ($\vec{1}_\|$) to the magnetic field.

For the sake of simplicity, we neglect the effects of the ambipolar perpendicular electric field for non-conducting walls and consider that the Diffusion term is uniform across the plasma, and simply defined as:

$$\mathcal{D}' = \begin{bmatrix} D_\perp & 0 \\ 0 & D_\| \end{bmatrix} ; \Theta = \frac{D_\|}{D_\perp} \tag{2}$$

Where Θ is the *diffusion coefficient ratio* and is the main parameter in this study, as it will determine the rate of numerical diffusion. Formally, this equation may be expressed in the way of the classical diffusion equation, taking into account the flux vector Γ and strictly positive diffusion coefficients, as:

$$\frac{dn}{dt} = \nabla' \cdot \left[\mathcal{D}' \cdot \nabla' n\right] = \nabla' \cdot \vec{\Gamma'} = \nabla' \cdot \begin{bmatrix} \Gamma_{x'} \\ \Gamma_{y'} \end{bmatrix} \tag{3}$$

[a] http://aero.uc3m.es/ep2/

The numerical diffusion problem arises when the diffusion equation (Eq. (3)) is discretized in a coordinate system which is not aligned with the perpendicular and parallel directions of the magnetic field, such as a cartesian coordinate system for a randomly aligned magnetic field (Fig. 2). For simplicity we will consider that magnetic field lines are straight (although the problem is generalizable to a "curved" field) and that the magnetic versors ($\vec{1}_\perp$, $\vec{1}_\parallel$) are rotated an angle α with respect to the cartesian system.

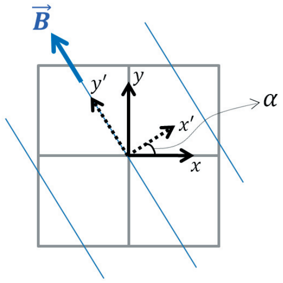

Figure 2. Regular structured mesh with angled Magnetic field

The rotation matrix $\mathcal{R}$ allows allows for transforming Eq. (3) into cartesian coordinates by using the relations:

$$\mathcal{R} = \begin{bmatrix} \cos\alpha & -\sin\alpha \\ \sin\alpha & \cos\alpha \end{bmatrix}; \vec{\Gamma} = \mathcal{R}\cdot\vec{\Gamma'}; \nabla' n = \mathcal{R}\cdot\nabla n \tag{4}$$

Which results in a diffusion equation in cartesian coordinates which satisfies:

$$\frac{dn}{dt} = \nabla\cdot\left[\mathcal{R}^{-1}\mathcal{D}'\mathcal{R}\cdot\nabla n\right]; \tag{5}$$

$$\mathcal{D} = \mathcal{R}^{-1}\mathcal{D}'\mathcal{R} = \begin{bmatrix} D_\perp\cos^2\alpha + D_\parallel\sin^2\alpha & \left(D_\parallel - D_\perp\right)\cos\alpha\sin\alpha \\ \left(D_\parallel - D_\perp\right)\cos\alpha\sin\alpha & D_\parallel\cos^2\alpha + D_\perp\sin^2\alpha \end{bmatrix}$$

Integrating over each mesh element volume and applying the Gauss divergence theorem in Eq. (5) we reach an expression which must be satisfied for every mesh element:

$$\int_V \frac{dn}{dt} = \oint_A \begin{bmatrix} (D_\perp\cos^2\alpha + D_\parallel\sin^2\alpha)\frac{\partial n}{\partial x} + \left(\left(D_\parallel - D_\perp\right)\cos\alpha\sin\alpha\right)\frac{\partial n}{\partial y}\right) \\ \left(\left(D_\parallel - D_\perp\right)\cos\alpha\sin\alpha\right)\frac{\partial n}{\partial x}\right) + (D_\parallel\cos^2\alpha + D_\perp\sin^2\alpha)\frac{\partial n}{\partial y} \end{bmatrix}\cdot d\overrightarrow{A} \tag{6}$$

Equation (6) is analogous to the one derived by Wirz[8] and demonstrates how numerical diffusion appears in non-aligned meshes. Indeed, the Diffusion term expressed in cartesian coordinates will be responsible for the "cross-contamination" we mentioned earlier, due to the fact that, in general, $D_\parallel \gg D_\perp$; numerical diffusion appears even when the diffusion coefficient ratio is $\Theta \to \infty$ ($D_\perp = 0$), the plasma is perfectly confined), this may be simply understood through the sketch in Fig. 3: first, the cross-diffusion term induces a transfer of mass between contiguous cells when none should occur (Fig. 3a)); second, for $\Theta \to \infty$ magnetic field lines are impermeable to mass-flow, and yet, because of the iterative nature of numerical solutions, mass will "creep" through the mesh cells (Fig. 3b)) due to the lack of alignment between the mesh and the magnetic field.

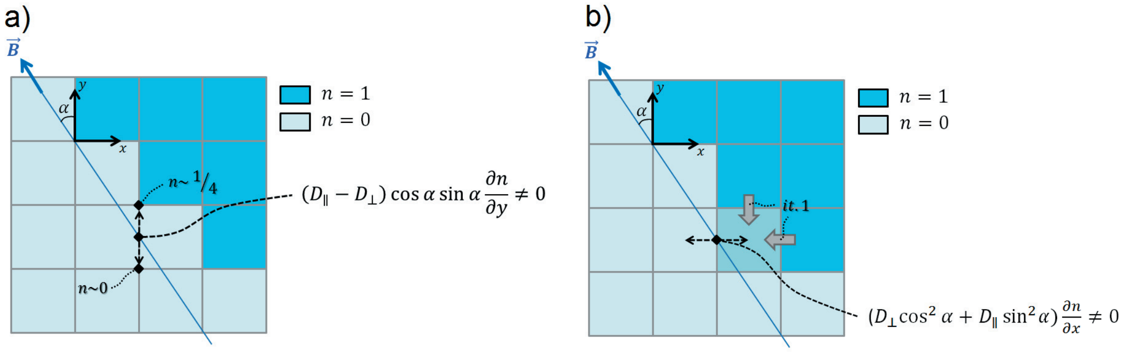

Figure 3. Sketch on numerical diffusion

A. Case Results

Equation (6) may be solved using the Finite Volume Method (FVM), which is also utilized in NOMADS, as it provides a formulation of the problem in conservative form (versus the weak forms of the Finite Element and Finite Differences Methods); for a particular mesh volume element, this equation is discretized for each element by an *explicit Euler method* as:

$$V_i \frac{n_{e,i}^{t+\triangle t} - n_{e,i}^{t}}{\triangle t} =$$
$$= \sum_j \left(\left[\begin{array}{c} (D_\perp \cos^2\alpha + D_\parallel \sin^2\alpha)\frac{\partial n}{\partial x} + \left((D_\parallel - D_\perp)\cos\alpha \sin\alpha\right)\frac{\partial n}{\partial y} \\ \left((D_\parallel - D_\perp)\cos\alpha\sin\alpha\right)\frac{\partial n}{\partial x}\right) + (D_\parallel \cos^2\alpha + D_\perp \sin^2\alpha)\frac{\partial n}{\partial y} \end{array} \right] \Bigg|_{f,j} \cdot dA_{f,j}\vec{n}_{f,j} \right) \tag{7}$$

Where "e,i" represents the i^{th} *element* and "f,j" the j^{th} facet of that element. Derivatives on the regular structured mesh are approximated by a central differencing scheme (in the same way as shown in Ref. 8), based on the sketch in Fig. 4 as:

$$\frac{\partial n}{\partial x} \approx \frac{n_2 - n_1}{\triangle x}; \frac{\partial n}{\partial y} \approx \frac{\frac{n_1+n_2+n_3+n_4}{4} - \frac{n_1+n_2+n_5+n_6}{4}}{\triangle y} \tag{8}$$

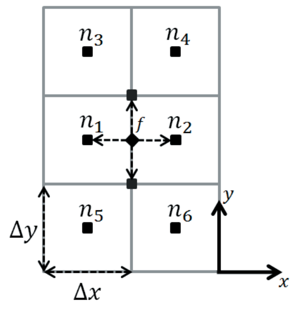

Figure 4. Central Differences schematic

Equation (7) is applied to each element leading to a system of equations contained in a sparse matrix; we may use numerical solvers to obtain the evolution of the anisotropic diffusion problem (with $\Theta = {}^{D_\parallel}/_{D_\perp}$) for the "less-formal" *non-permeable walls* under a magnetic field forming an angle α with the cartesian system. Fig. 5 shows the system evolution for $\alpha = -45^o$ and $\Theta \to \infty$ which, as expected, presents numerical diffusion (the *red line* in the figure represents a magnetic field line and as such should be impermeable to the plasma given the initial conditions).

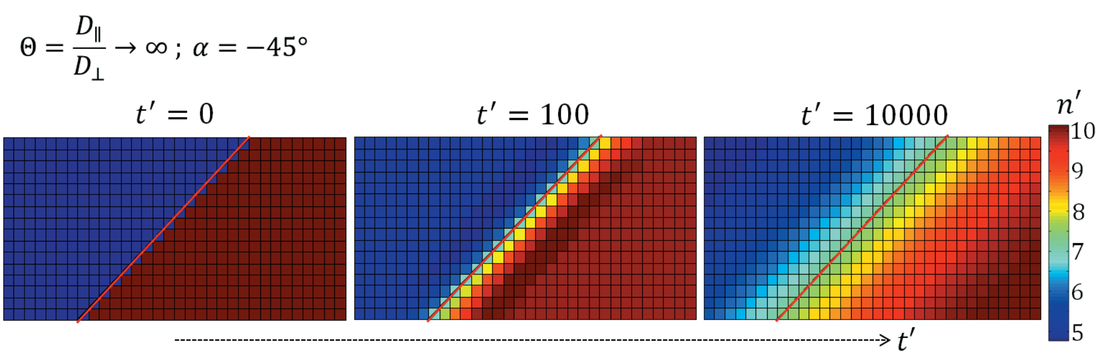

Figure 5. Numerical Diffusion in anisotropic diffusion problem (variables are non-dimensional)

Errors committed due to numerical diffusion for the with $\Theta \rightarrow \infty$ case with different α and different number of mesh elements are quantified through the average error density for the elements in the "low density" zone (left of the red line in Fig. 5), considering that the plasma should be perfectly confined:

$$\langle error(t) \rangle = \frac{1}{N_{elem}} \sum_{i=1}^{N} \frac{|n_i(t) - n(t=0)|}{n(t=0)} \tag{9}$$

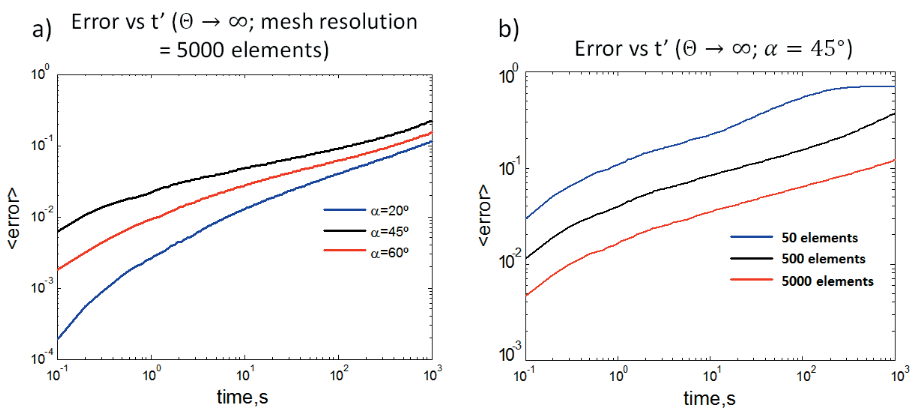

Figure 6. a) Error vs. t' for different α; b) Error vs. t' for different mesh resolution

Figure 6 quantitatively shows the evolution of the error due to numerical diffusion in our problem; however, we wish to seek a more qualitative result in order to assess the effects of numerical diffusion. For this reason we propose the concept of *effective diffusion coefficient ratio* Θ_{eff}: for a given simulation domain, mesh resolution, number of elements in the initial low/high plasma density regions, α and Θ, we study an analogous problem in which the mesh and magnetic fields are aligned; the $\Theta_{\text{"}aligned\text{"}}$ for the "aligned" mesh which provides an equivalent *diffusive mass flux* (between the different plasma density regions) to the "non-aligned" problem is the Θ_{eff}.

	$\Theta_{eff} \sim ...$	$\Theta \to \infty$	$\Theta = 100$	$\Theta = 10$
Mesh resolution = 50 elements	$\alpha = 20^o$	~ 5	~ 4	~ 3
	$\alpha = 45^o$	~ 5	~ 5	~ 3
	$\alpha = 60^o$	~ 5	~ 5	~ 3
Mesh resolution = 500 elements	$\alpha = 20^o$	~ 20	~ 15	~ 5
	$\alpha = 45^o$	~ 25	~ 15	~ 5
	$\alpha = 60^o$	~ 20	~ 15	~ 6
Mesh resolution = 5000 elements	$\alpha = 20^o$	~ 50	~ 25	~ 8
	$\alpha = 45^o$	~ 50	~ 30	~ 8
	$\alpha = 60^o$	~ 50	~ 30	~ 7

Table 1. ***Effective Diffusion Coefficient ratio*** **(Θ_{eff}) for different mesh resolutions, alignment of the magnetic field (α) and diffusion coefficient ratios (Θ)**

Table 1 presents results for the effective diffusion coefficient with different parameter sets for the problem described by Eq. (6), solved through an explicit Euler/FVM discretization. Results are in line with both Ref. 3 and Ref. 4: numerical diffusion leads to a reduction in the anisotropicity of the system, errors are more or less independent to the misalignment of the magnetic field to the mesh (for the explored sets); they are however very noticeable for lower resolution meshes and only partially recoverable through refinement for the high anisotropicity cases.

III. Meshing strategies for MFAMs

A stationary MFAM may be built when the magnetic field in the simulated domain can be considered to be both irrotational ($\nabla \times \vec{B} \approx 0$) as well as solenoidal ($\nabla \cdot \vec{B} = 0$) and stationary ($\frac{\partial \vec{B}}{\partial t} = 0$). Indeed, the irrotational approximation is valid whenever the effect of the plasma discharge over the magnetic field is small compared to the field generated by the magnetic circuit.

The above relations allow us to derive the magnetic stream-line function λ and the magnetic potential function σ, which can be integrated in a typical *axisymmetric* simulation domain (Fig. 7) to obtain a curvilinear system of "magnetic" coordinates:

$$\nabla \cdot \vec{B} = 0 \to \nabla^2 \lambda = 0 \to \frac{\partial \lambda}{\partial r} = -rB_z; \frac{\partial \lambda}{\partial z} = rB_r \tag{10}$$

$$\nabla \times \vec{B} \approx 0 \to \nabla \sigma = \vec{B} \to \frac{\partial \sigma}{\partial r} = B_r; \frac{\partial \sigma}{\partial z} = B_z \tag{11}$$

Lines of constant λ always follow the local direction of the magnetic field ($\vec{1}_{\|}$) and lines of constant σ are always in the perpendicular direction to the magnetic field ($\vec{1}_{\perp}$); it is precisely these "isolines" through which we define the non-structured MFAM.

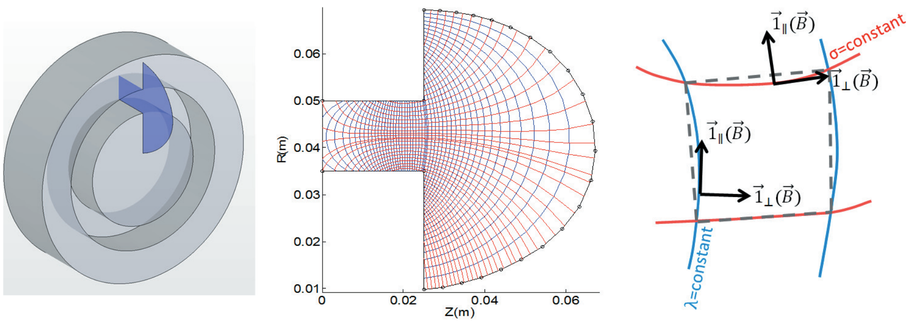

Figure 7. Simulation domain in an SPT-100 HET, Isoline mesh (MFAM) for the SPT-100 magnetic topology (axisymmetric domain) & detail of mesh element

The solution to a highly anisotropic problem posed in the local versor system defined by the magnetic field, with respect to the magnetic coordinates cannot, by definition, show numerical diffusion as understood here (as it would be the equivalent of solving the problem defined by Eq. (1)); however, building a robust mesh in which to solve the problem presents a number of challenges which need to be assessed through different strategies and functionality in the meshing algorithm.

Specifically, issues arise regarding mesh quality, mainly at the domain boundaries; Araki[5] tackles these by sacrificing the MFAM configuration in the boundary elements (and in the elements adjacent to those), choosing to relocate node positions to improve quality. The argument here is that poor mesh quality in the MFAM boundaries leads to errors in the numerical solution which are, at least, comparable to numerical diffusion.

This discussion is reserved for Section V, however, focusing on improvement of mesh quality, correct handling of gradient reconstruction and the implementation of a conservative method, such as the FVM, should allow us to correctly make use of the MFAM across the domain and contain the issue of numerical diffusion with little error specific to the non-structured mesh.

A. Meshing algorithms

A working Mesh Generator, has been built for the NOMADS platform. It performs the following tasks:

- Obtains the magnetic field in the selected simulation domain
- Integrates λ and σ in the domain (this is done over an initial structured cartesian "dummy" mesh)
- Selects λ and σ isolines (contour levels)
- Corrects isolines if required
- Builds the MFAM using the selected isolines; mesh information is stored by elements, facets, nodes, etc.

Two main concerns arise when building the MFAM: first, as the magnetic field is not constant in the domain, picking the contour levels of λ and σ to ensure that lines are correctly spaced requires careful consideration; this is specially true whenever singular points ($\left|\vec{B}\right| = 0$) or local minima appear in the domain: because of low magnetic field strength, there is a smaller variation of λ and σ values around these regions than there is in regions of high magnetic field strength, thus dedicated contour levels must be added in order to avoid excessively large mesh elements. Second, the mesh is determined by the topology of the magnetic field, with the user only being able to "adjust" which contour levels are picked, this implies that we have little control over where the isolines will intersect with the domain boundaries, leading to *low quality boundary elements*.

1. *Contour level initial selection*

The user starts by selecting the number of contour levels of λ and σ which will populate the simulation domain. The Mesh Generator then uses one of various algorithms in order to generate correctly spaced isolines in the mesh (picking specific contour level values), these allow the user to explore the best meshing methodology for the particular problem at hand. The algorithms, or "spacing methods", implemented are:

Smoothing The values for λ and σ are sorted and smoothed using a local regression method which applies weighted least squares and 2nd degree polynomial models; we obtain a correlation between the magnetic coordinate value and the "number" of instances it appears in the domain. We then evenly distribute the number of contour levels selected by the user over the correlation, which provides us with contour level values with a good spatial distribution, independent of the local rate of variation of the magnetic coordinate:

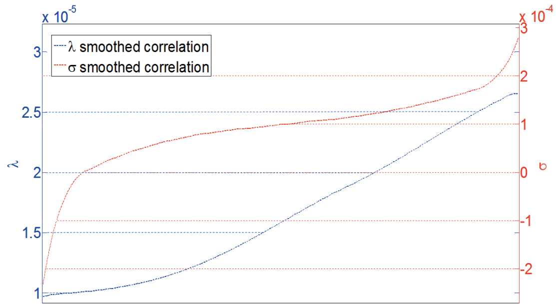

Figure 8. Evenly distributed contour levels based on λ& σ correlations

Logarithmic Obtains logarithmically spaced values for the magnetic coordinate between the maximum and minimum values resulting from the integration; this biases the selection of contour levels toward smaller values (associated with regions of lower magnetic field intensity), avoiding incorrect spacing around high magnetic field intensity regions.

Exponential-stretching This method was proposed by Araki[5] to deal with magnetic field topologies which contained singular regions and/or high ratios of maximum to minimum field strength. For either of the magnetic coordinates (characterized here as ψ), the n_ψ contour levels are obtained from:

$$\begin{cases} \psi_q = \psi_{min} \frac{\exp\left(\frac{q_0 - q}{q_0 - 1}\alpha_\psi\right) - 1}{\exp(\alpha_\psi) - 1} \text{ for } q < q_0 \\ \psi_q = \psi_{max} \frac{\exp\left(\frac{q - q_0}{n_\psi - q_0}\alpha_\psi\right) - 1}{\exp(\alpha_\psi) - 1} \text{ for } q > q_0 \\ q_0 = int\left(n_\psi \frac{\psi_{min}}{\psi_{max} - \psi_{min}}\right); \psi(q_0) = 0 \end{cases} \tag{12}$$

which implies obtaining the contour levels by exponentially stretching from $\psi = 0$ to positive and negative values of the magnetic coordinate; α_ψ is the "stretching parameter", which is specified as an input.

"Expanded"-exponential-stretching Based on Araki's method but with an expanded functionality to account for the possibility of having multiple singular points; also allows for specific control of the stretching method around these points (including adding "fractional" levels for fine tuning of the mesh elements and incorporating the contour lines which cross the singular points).

Examples of the meshing algorithms for a typical HET magnetic field the simulation domain are shown in Fig. 9; the method proposed by *Araki* was found to *be consistently more robust in achieving initial meshes with good spacing properties* for the particular magnetic topologies put to trial.

2. *Contour level manual correction*

However the initial selection of λ and σ isolines is performed, the mesh will present issues with regards to spacing and boundary elements; in case of the latter, issues come in the form of elements with a variable number of facets (three, four, or five), in comparison to interior elements which are always four-sided, the appearance of some small area elements, elements with large aspect ratios (where the boundary facet is very small compared to the others), etc. (refer to Fig. 10)

In order to improve the quality of the MFAM, and also to provide a tool for fine tuning of the mesh, further functionality has been implemented into the Mesh Generator in order to "manually" correct λ and σ isolines; a Graphical User Interface which allows for manually deleting and adding isolines from the simulation domain.

IV. Mesh Regularity: Geometric Quality and Gradient Reconstruction in MFAMs

Recent studies on the effects of "mesh regularity", such as the one performed by Diskin,[9] indicate that the quality of the mesh cannot be truly assessed without taking into account the nature of the problem, the numerical discretization approach and the expected computational output, in addition to purely geometric quality indicators. Particularly, the FVM method is referred to by Diskin[9] as being *resilient* against the effects of "non-regularity" in non-structured meshes, which provides an additional level of confidence for the argument of utilizing the MFAM approach.

We discuss here results for MFAM quality (geometric and gradient based) without delving into their effects over a particular problem. The understanding is that, however resilient, errors in terms of discretization, interpolation and gradient calculation (which can be linked both to geometric properties of the mesh and to the methods used for gradient reconstruction) may plague our solution; therefore it is best to minimize these issues from the start.

A. Geometric Mesh Quality

The different possibilities offered by the meshing algorithms and the fine tuning through *manual correction* allow the user to iterate through MFAMs with increasingly better geometric quality properties; non withstanding, high quality meshes will always be difficult to achieve due to the restriction of using isolines which are defined by the magnetic topology over "arbitrary" simulation domains.

Qualitatively, geometric quality is described through the following set of element properties:

$$\begin{aligned} smoothness &= \frac{max(A_{element}, A_{adjacent})}{min(A_{element}, A_{adjacent})} \\ aspect\ ratio &= \frac{max(facet{-}length_{element})}{min(facet{-}length_{element})} \\ skewness &= max\left[\frac{\theta_{max}-\theta_e}{\text{180ï¿œ}-\theta_e}, \frac{\theta_e-\theta_{max}}{\theta_e}\right] \end{aligned} \tag{13}$$

Where A represents the areas, *element* and *adjacent* represent, respectively, the element being considered and the elements adjacent to it, θ_{max} is the largest angle in the element polygon and θ_e is the angle in an equiangular polygon with the same number of sides as the element considered.

Large aspect ratios and smoothness may be intuitively understood to affect the interpolation of the solution and gradient reconstruction in the element faces (although this may be offset in part by using a "weighted" Least Squares (LSQR) method, see Section IV.B); skewness may be related to large errors for fluxes in facets which are nearly parallel.

In order to showcase how the functionality in the Mesh Generator allows us to improve the geometric quality of the MFAM, we compare two meshes through their quality statistics: one generated using the *smoothing* method with no manual correction and one generated using the *exponential stretching* method and manual correction of the mesh (Fig. 9). Figure 10 shows that we are able to partially recover better geometric quality properties in the mesh through the implemented functionality.

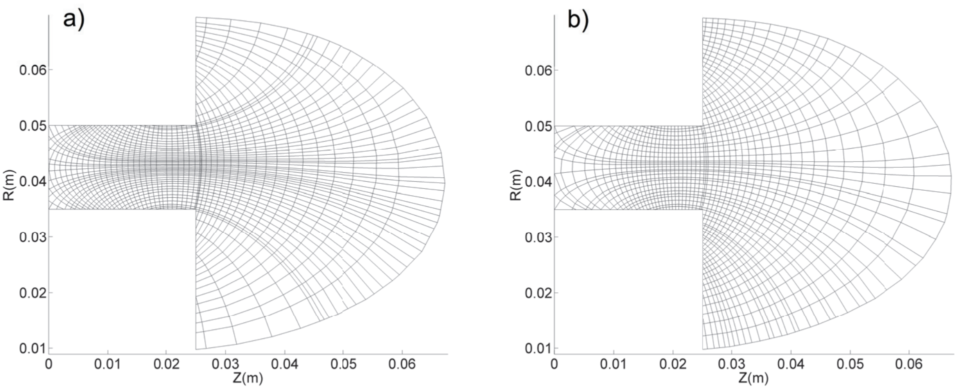

Figure 9. a) Smoothing method (no manual correction); b) Exponential Stretching method & manual correction (initial number of λ and σ isolines = 50)

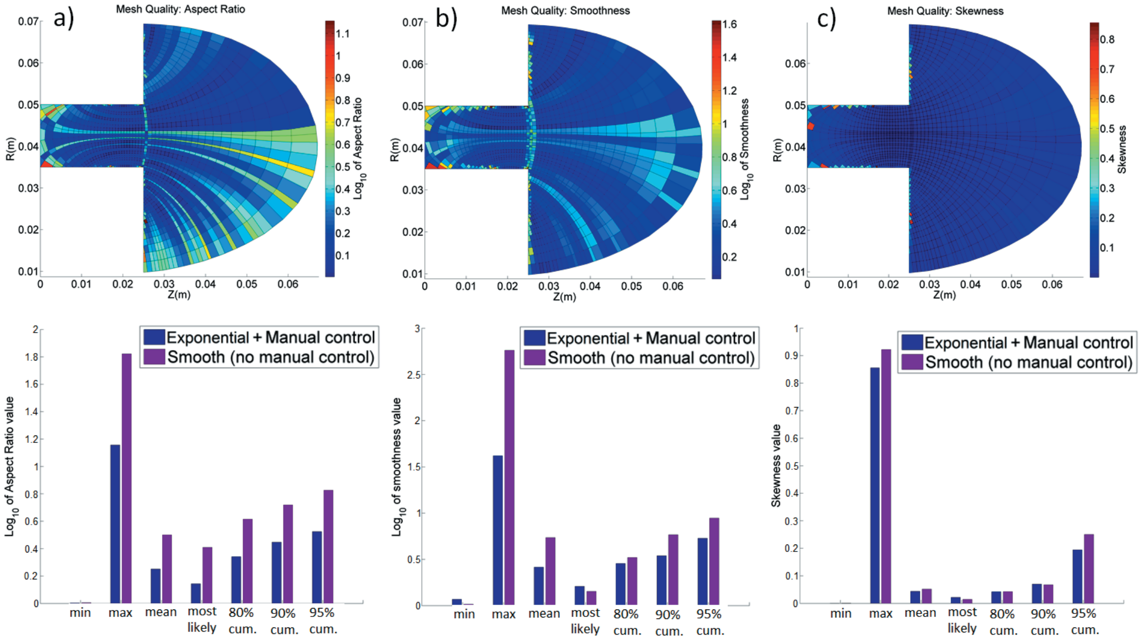

Figure 10. a) Aspect Ratios, b) Smoothness, c) Skewness; (top) 2D profiles in the mesh, (bottom) Comparison for mesh quality statistics between Exponential-Stretching method mesh and Smoothing method mesh -min., max., mean, most likely, 80% cumulative, 90% cumulative, 95% cumulative-

B. Gradient Reconstruction

Gradient reconstruction (GR) is required in "cell-centered" ("element-centered") FVM schemes in order to obtain partial derivatives at the element facets. For regular structured meshes, such as the one employed in Section II.A, central or upwind differencing schemes retain an acceptable order of accuracy; however, whenever dealing with non-structured meshes, such as the MFAM, higher order differencing schemes become necessary.

Both Diskin[9] and Sozer[10] review the use of the Green-Gauss (GG) and the LSQR (both Weighted -WLSQR- and Unweighted -ULSQR-) methods in terms of order of accuracy for GR; Sozer also performs analysis on additional methods, showcasing that, while consistency in the GG and LSQR methods might vary with mesh regularity, other methods tend to have lower orders of accuracy.

We have chosen the WLSQR method for GR in the MFAM; particularly, we use an equivalent to the WLSQR Face Interpolation -WLSQRFI- method described by Sozer[10] as "cell-centered" FVM discretization usually requires gradients at the element facets. The resulting set of equations (based on the Taylor series expansion) determine the value of any function ϕ at the facet center, as well as derivatives and cross-derivatives, from the value of ϕ at a number of *stencil points* and the set of *weights* assigned to them; stencil points are chosen as the centers of the surrounding elements and weights are typically functions of the inverse distance, element areas, etc. (or simply equal to 1 if we wish to recover the ULSQR).

The WLSQR method offers a high level of flexibility to "tune" the quality of GR in a particular mesh: we may choose both the appropriate weights and order of the Taylor series (which can be *done independently for interior and boundary elements in the MFAM*[b], as part of the functionality implemented in our platform).

The main set-back is that we do not know, a-priori, the shape of the function ϕ. We will show that the accuracy of GR depends greatly on both the particular type of function and on the selection of the parameters which confer the flexibility to the method; Fig. 11 shows errors committed by numerical GR, using *inverse-distance weighting* for *Taylor series expansion up to 2nd order (9 stencil points)*, in the "exponential-stretching" mesh (Fig. 9b)) for the following analytical trial functions:

[b]Allowing for a sort of "hybrid mesh", which, as concluded by Sozer,[10] might offer the best compromise between GR methods.

$$
\begin{aligned}
\phi_1 \sim &\quad \lambda^2 + \sigma^2 \\
\phi_2 \sim &\quad \lambda^3 \cdot \sigma^3 \\
\phi_3 \sim &\quad \sin\lambda \cdot \cos\sigma
\end{aligned}
$$

Where λ and σ are the magnetic coordinates defined in Eq. (10) and (11). Figure 12 shows variation in error statistics for different weights and Taylor expansion orders for the different trial functions.

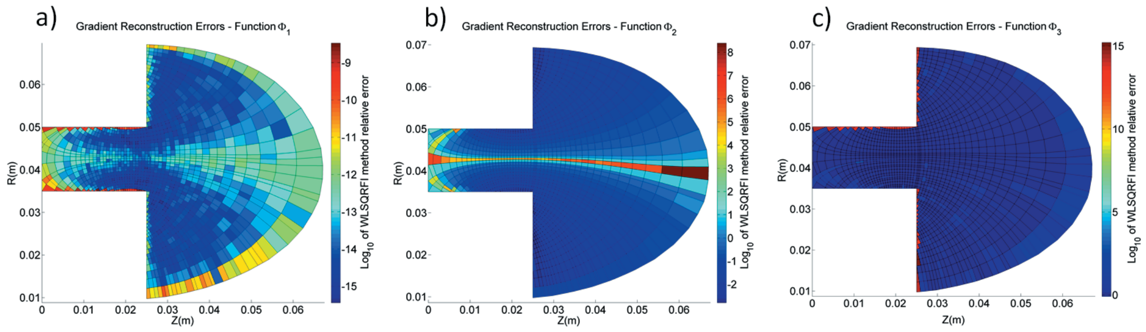

Figure 11. $\log_{10}$ **of relative errors in the WLSQR method -9 stencil points, inverse-distance weighting for a)** ϕ_1**; b)** ϕ_2**; c)** ϕ_3 **(elements are colored according to the worst GR error for their respective facets)**

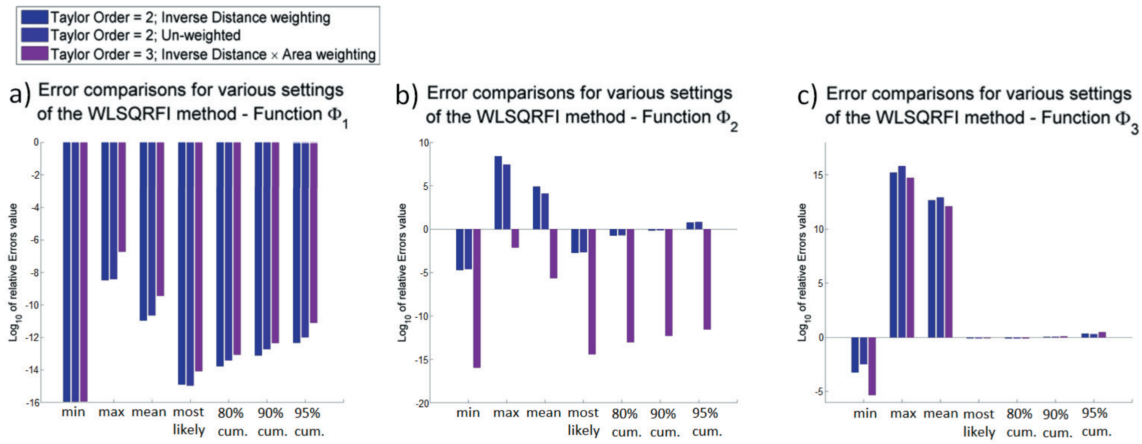

Figure 12. Comparison of GR errors for various WLSQR method parameters (Taylor order = 2 & inverse-distance weighting; Taylor order = 2 & unweighted; Taylor order = 3 -16 stencil points- & inverse-distance × area weighting) for a) ϕ_1**; b)** ϕ_2**; c)** ϕ_3

Figure 11 showcases a certain correlation between low geometric quality regions and large errors in gradient reconstruction, specifically in boundary elements (poor skewness and smoothness) and poor aspect ratio elements. In terms of the LSQR method, two aspects become clear: first, selection of the parameters can mean the difference between unacceptable and acceptable errors in the calculation of gradients (as inferred from Fig. 12b)). Second, a good accuracy GR cannot be recovered for certain function-mesh combinations, as shown in Fig. 12c): function ϕ_3 presents relative errors $\gtrsim 1$ because the mesh does not provide enough *resolution* for the LSQR method to correctly obtain the function gradients for the particular wavelength of the function (it is worth noting that a similar issue will arise in a regular structured mesh without sufficient resolution).

We can conclude that a compromise must be made between the Taylor series order (which determines the number of stencil points), the resolution of the mesh and our previous knowledge of the behavior of functions and variables in the domain in order to ensure good accuracy in the gradient reconstruction.

V. MFAM Benchmark results for the anisotropic diffusion problem

One of the main arguments against the use of MFAMs is that the numerical errors due to lack of mesh "regularity" are, potentially, of the same order than those caused by numerical diffusion in a regular structured mesh. This section presents a "benchmark" simulation to compare these errors: the numerical problem presented in Section II.A may be generalized to take into account a curved magnetic field (variable alignment of the magnetic field directions -variable α- with respect to the cartesian coordinates), so that a comparison between meshes is possible.

In Fig. 13 we compare solutions in both regular and aligned meshes (with the same number of elements) for a magnetic field generated by a current traversing a wire and a simulation domain both arbitrarily large and at an arbitrary distance from the wire; again, the main parameter in the simulation is $\Theta = {}^{D_\parallel}/{}_{D_\perp} = 10$ and the MFAM simulation is solved with a WLSQ method with Taylor order $= 1$ (up to the first order cross derivatives) and inverse-distance weighting (which was found to produce the lowest GR errors for this particular case). Figure 14 shows the average density evolution in the initial low density region (pictured at $t' = 0$ in Fig. 13) in both meshes and accounts for the difference between the two solutions due to numerical errors.

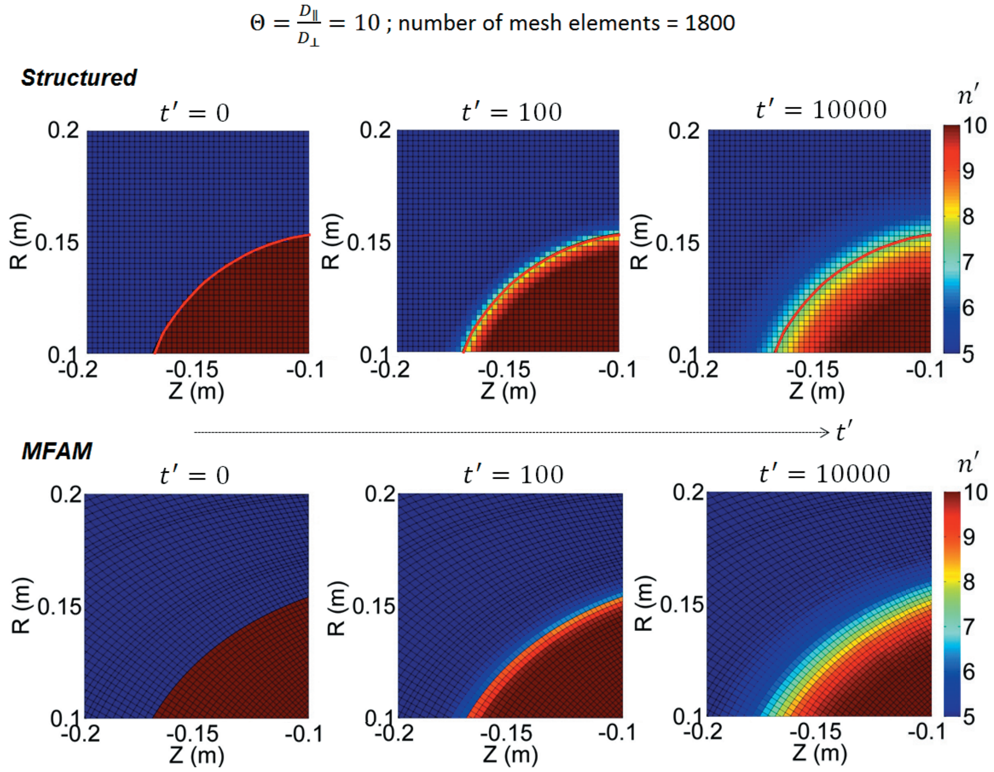

Figure 13. Anisotropic diffusion problem solution in structured (top) and MFAM (bottom) meshes

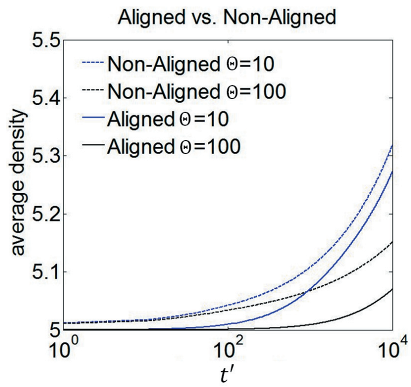

Figure 14. Evolution of average density due to diffusion @ initial "low density" region for Structured and MFAM meshes (different Θ values)

Typical numerical discretization errors appear in MFAM elements due to issues in gradient reconstruction, but not due to numerical diffusion. As evidenced by the results, these errors are small in comparison to global errors caused by numerical diffusion in the structured mesh and imply that both solutions will diverge for sufficiently large times.

Considering that the simulation for the MFAM is solving the *exact* diffusion problem, albeit with the introduction of numerical discretization errors, it is understood that, in general, MFAMs offer a solution which is more consistent with the actual evolution problem than the structured mesh for similar mesh refinement.

An additional discretization error in MFAMs appears because magnetic stream-lines and lines of constant magnetic scalar potential lose their local curvature when mesh elements are generated (Fig. 7), as element facets are always straight. This error is difficult to quantify, although it is presumably small and, formally, does not affect the validity of applying a purely diagonal second order Diffusion term (i.e., no numerical diffusion appears because of it).

VI. Conclusions

The previous sections have shown that large anisotropicities in the diffusion problem are difficult to recover in a regular structured mesh without extensive refinement of the mesh, which would typically involve large computational resources to solve the problem accurately. In MFAMs this problem disappears, by definition, although numerical discretization errors are still present.

For smaller anisotropicity levels, the relatively smaller numerical diffusion errors might be traded-off against the difficulties of using the non-structured mesh: the understanding that gradient reconstruction in a MFAM might cause large errors for certain types of solutions (if the method parameters are incorrectly selected) and the general added difficulty of handling a non-structured problem, purely from a coding perspective.

In this regard, we argue that plasma discharges in electric propulsion devices happen under complex magnetic topologies (with distinct regions of confinement) and depend greatly on the operating parameters of these devices; this means that prior knowledge of the anisotropicity level in the different transport terms of the governing equations is difficult to attain. Consequently, arbitrarily large refinement of a structured mesh might be needed to deal with numerical diffusion. Furthermore, issues in gradient reconstruction may also appear in structured meshes if mesh resolution and the order of the method are not correct; in the case of MFAMs, various strategies have been presented in this work in order to provide additional confidence on our capability to deal with errors introduced by "non-regularity" in the mesh.

Considering all of the above, we conclude that the use of MFAMs for the simulation of magnetically confined discharge plasmas (or specific populations within them), modeled as highly anisotropic fluids, in electric propulsion devices, provides a distinct advantage in bounding numerical errors in the solution, as long as specific challenges in these meshes are taken into account.

Future work will be oriented toward adding "attractor points" in MFAM meshing strategies for additional control over mesh refinement as well as understanding the possible benefits of mesh quality improvement methods in boundary elements for problems with non-trivial boundary conditions.

Furthermore, the authors are continuing with development on the NOMADS platform; related to numerical simulations, it is expected that the extent of errors caused by lack of mesh regularity in the MFAM may be quantified for plasma discharges in characteristic conditions of electric propulsion devices.

VII. Acknowledgments

This work has been supported by Spain's R&D National Plan, grant number ESP2013-41052-P.

Additionally, the authors would like to acknowledge Samuel Araki and Richard Wirz for their description of the *exponential stretching method* for contour level selection in MFAM meshing, as it consistently provides the best spacing properties amongst the surveyed algorithms.

References

[1]R. Marchanda, M. Dumberrya, "CARRE: a quasi-orthogonal mesh generator for 2D edge plasma modeling", Computer Physics Communications, Volume 96, Issues 2–3, Pages 232–246, August 1996

[2]Ioannis G. Mikellides, Ira Katz, Richard R. Hofer, Dan M. Goebel, Kristi de Grys, and Alex Mathers, "Magnetic shielding of the channel walls in a Hall plasma accelerator", Physics of Plasmas 18, 2011

[3]Anderson, D. V., "Axisymmetric Multi-fluid Simulation of High Beta Plasmas with Anisotropic Transport Using a Moving Flux Coordinate Grid," Journal of Computational Physics, Vol. 17, pp. 246-275, 1975.

[4]Meier, E. T., Lukin, V. S., and Shumlak, U., "Spectral Element Spatial Discretization Error in Solving Highly Anisotropic Heat Conduction Equation," Computer Physics Communications, Vol. 181, pp. 837-841, 2010.

[5]Samuel J. Araki, Richard E. Wirz, "Magnetic Field Aligned Mesh for Ring-Cusp Discharge Chambers", 50th AIAA/ASME/SAE/ASEE Joint Propulsion Conference, July 2014

[6]Diego Escobar and Eduardo Ahedo, "Two-Dimensional Electron Model for a Hybrid Code of a Two-Stage Hall Thruster", IEEE Transactions on Plasma Science, Vol. 36, No. 5, October 2008

[7]Albert Simon, "Diffusion of Arc Plasmas across a Magnetic Field", 2nd Geneva Conference on Peaceful Uses of Atomic Energy, Vol. 32 p. 366, Geneva, 1959

[8]Wirz, R. E., "Discharge Plasma Processes of Ring-Cusp Ion Thrusters", Ph.D. thesis, California Institute of Technology, Pasadena, California, 2005.

[9]Boris Diskin, James L. Thomas, "Effects of mesh regularity on accuracy of finite-volume schemes", 50th AIAA Aerospace Sciences Meeting including the New Horizons Forum and Aerospace Exposition, January 2012, AIAA 2012-0609

[10]Emre Sozer, Christoph Brehm and Cetin C. Kiris, "Gradient Calculation Methods on Arbitrary Polyhedral Unstructured Meshes for Cell-Centered CFD Solvers", 52nd Aerospace Sciences Meeting, 2014